ORIGINAL RESEARCH ARTICLE

Thermo-Mechanically Assisted Grain Growth in Ti6Al4V Fabricated Using the Powder Bed Additive Manufacturing During High-Temperature Mechanical Testing

LEILA LADANI, JAFAR RAZMI, and MD. JAMAL MIAN

High-temperature mechanical behaviors of metal alloys and the underlying microstructural variations responsible for such behaviors are important areas of interest for many industries particularly in their high-temperature applications. Transformation of grains which occur both during metal powder bed fusion additive manufacturing processes due to variation of thermal gradient and cooling rates, and afterward during different thermomechanical loads that parts experience in their specific applications, could also impact its mechanical properties both at room and high temperatures. This study focuses on in-depth analysis and understanding of how the grain structures of electron beam powder bed fusion (EB-PBF) Ti6Al4V alloy changes during high-temperature mechanical load, due to the interacting mechanisms. Mechanical testing is conducted for EB-PBF parts made at different build orientations up to 600 °C. Microstructural analysis using electron backscattered diffraction (EBSD) is conducted on samples before and after high-temperature mechanical testing to understand the interacting impact that temperature and mechanical load have on the activation of deformation mechanisms. EBSD analysis showed both grain size and grain orientation to be dependent on the build orientation. Mechanical testing at high temperature showed softening behavior especially from 400 °C to 600 °C temperature. Additionally, anisotropic behavior was observed which is associated with volume ratio of β phase as well as the anisotropic grain formation. Some grain coarsening was observed at higher test temperatures. Additional changes in misorientation angle and certain preferred grain orientation that varies with temperature signifies activation of geometric deformation mechanism.

https://doi.org/10.1007/s11661-023-06989-y

I. INTRODUCTION

Ti6Al4V alloy has numerous applications in various industries such as aerospace, automobile, biomedical, and nuclear, primarily because of its high strength, lightweight, high melting temperature, and excellent corrosion resistance. In addition to that, this $\alpha + \beta$ alloy has become an exceptional choice for different structural components utilized in various high-temperature environments, for instance inside jet engines, nuclear reactors, and heat exchangers.[1,2] However, producing and shaping this alloy using conventional techniques is challenging because of its high melting temperature and its high strength. Powder bed fusion (PBF) additive manufacturing (AM) processes have shown outstanding prospects in terms of fabricating near net shape Ti6Al4V parts with minimal waste and a very short lead-time.[3] Despite having these advantages over traditional methods, PBF AM processes also have some considerable challenges. For example, the PBF AM processed metal parts normally contain distinct microstructure, significant mechanical anisotropy, various inherent manufacturing defects such as porosity (lack of fusion, keyhole), and high surface roughness.[4–6] The distinct microstructural features can translate into vastly different mechanical behavior. When PBF AM parts are used at different high-temperature environments, various thermo-structural phenomena can affect the inherent microstructure and the subsequent properties and performance of the components. The large variability seen in different PBF

LEILA LADANI and MD. JAMAL MIAN are with the School for Engineering of Matter, Transport and Energy, Ira A. Fulton Schools of Engineering, Arizona State University, Tempe, AZ 85281; JAFAR RAZMI is with the School of Sustainable Engineering and the Built Environment, Ira A. Fulton Schools of Engineering, Arizona State University, Tempe, AZ 85281. Contact e-mail: Leila.j.ladani@gmail.com
Manuscript submitted June 28, 2022; accepted January 22, 2023.

Published online: 18 February 2023

techniques has been a hurdle for manufacturers in adapting the technologies.[7]

Metal PBF mainly utilizes either laser or electron beam to melt the powder base materials. Both methods have been found very effective as viable manufacturing techniques in producing bulk components with complex geometries.

Because of the inherent differences between the physics of electron beam and laser, Ti6Al4V parts manufactured by these two processes demonstrate slightly different resultant microstructural features, mechanical properties and performances. Selective Laser Melting (SLM) technique has shown to produce Ti6Al4V parts with a distinct α'martensitic alpha phase, whereas the EBM processed parts normally consist of the α phase and the prior β phase on the alpha grain boundaries.[7,8] The main factor dictating the final microstructure is the temperature gradients during melting and solidification.. Both laser and electron beam cooling rates far exceed the conventional methods. EBM cooling rates experience during the process are shown in xxxx in an experiment and analysis done by NIST. This translates into a whole different set of scenarios that have not been investigated properly. EBM process uses a heated baseplate. Additional preheating steps are also used to raise the powder bed temperatures in between building each layer. Because of these factors, it is very likely that the parts remain at high temperatures for an extended period during build.

During the early solidification of the EBM processed Ti6Al4V melt pool, when the temperature remains higher than the β-transus temperature (980 °C), it initially solidifies into primary β grains speedily. These primary β grains, then convert into martensitic α phase due to rapid cooling rates. As the part remains at higher temperatures, it allows for transformation of the resultant martensitic α' phase into a combination of α phase (α colony, α basketweave) and β phase following a solid phase transformation at a slower cooling rate, as a result of a near-isothermal annealing process as induced by the elevated build temperature of around 700 °C.[9]

Additional observation in literature has shown the anisotropic microstructure and mechanical behavior in Ti6AL4V parts made using SLM or EBM. This anisotropy has been discussed in many different studies[5,10,11] and the underlying mechanisms are found to be the grain texture and columnar grain growth formation due to a similar mechanisms as epitaxial growth during the process.[5,12]

Most studies have focused on room temperature behavior. High temperature mechanical behavior has been reported by various researchers.[8,13–18] Various mechanisms have been found to be activated during high-temperature deformation resulting in softening behaviors. In the temperature range of 500 °C to – 850 °C which falls in the α phase field, the potential softening mechanisms are grain coarsening, elongation, rotation, platelet local shear deformation, and dislocation glide and climb.[18,19] On the contrary, during hot pressing at high temperature, adiabatic heating, and $\alpha \rightarrow \beta$ phase transformation (between temperatures 850 °C to 950 °C), dynamic recovery and dynamic recrystallization (DRX) (between temperatures 1000 °C to 1050 °C) have been identified as possible flow softening mechanisms by Ding *et al.*[13] The observed microstructural evolution was found to be impacted by the initial microstructure, hot working temperature, strain rate, and successive cooling rate. The different cooling rates also determine the morphology of the resultant α phase as Widmanstätten or acicular, equiaxed, plate-like, and basket weave. The adiabatic heating might raise the actual temperature of the sample and thus increase the softer β phase which is responsible for softening behavior of the sample. He *et al.*[14] also reported the dynamic recrystallization and globularization of α layers to be activated during hot deformation at temperatures higher than β-transus, resulting in microstructural evolution and softening of Ti6Al4V alloy. Dynamic α-grain coarsening was also observed to be activated during slow hot deformation and subsequent quenching at 500 °C and 600 °C.

The temperature during mechanical loading plays a significant role in controlling the evolution of the α and β phases. Additionally, mechanical deformation at high temperatures reduces the dislocation density due to the thermally activated dislocation motion resulting in softening behavior in the alloy.[17]

The microstructural evolution and related mechanical behaviors of traditionally produced Ti6Al4V alloy, during various thermomechanical processing and hot deformation, have been examined by various researchers. These studies have resulted in identifying various mechanisms responsible for certain mechanical behaviors. However, due to complexity associated with the microstructure containing multiple phases, variation of grain size and microstructure impacted by the manufacturing methods and variability in strain rate effect, the results of past studies may not be directly applicable to the parts made using EBM additive manufacturing method. Moreover, there are very limited works reported in the literature, according to the author's knowledge, focusing and analyzing high-temperature mechanical behavior and corresponding microstructural evolution of AM built Ti6Al4V alloy. Due to the critical role, Titanium alloy plays in high-temperature applications in aerospace and other industries.[20,21] Specifically, in aerospace industry, Ti6Al4V is often used for jet engines and gas turbine parts.[1] This study focuses on the high-temperature mechanical behaviors of Ti6Al4V parts built by EB-PBF up to 600 °C. The microstructural evolution and subsequent changes of texture, phase, preferred grain orientation, and sizes of the grains after tensile testing of the samples at different temperatures have been analyzed further, to understand potential softening mechanisms and their effect on the resultant mechanical properties. EBSD techniques have been used for the microstructural analysis of the sample after careful preparation of them using standard polishing processes, and to observe their respective microstructural evolution due to the applied thermomechanical loading.

II. SAMPLE PREPARATION

The sub-sized ASTM E8/E8M[22] dog-bone shape tensile test samples were produced using the Arcam® A2 EBM system.[23] Tensile test samples were fabricated at three different orientations, noted as top-built, side-built, and flat-built as shown in Figure 1. The flat-built and side-built samples are built at the horizontal layout and top-built samples are built at the vertical layout. The layers are stacked in thickness, width, and longitudinal directions for the flat-built, side-built and top-built samples, respectively. A cross-raster scanning strategy was used with a hatching distance of 200 μm, the layer thickness of 70 μm, incident beam size of 500 μm, scanning speed range of 0.5 to 15 m/s, and beam power range of 400 to 100 W for the printing process. A faster speed and lower power combination were used for preheating the powder bed and maintaining a high chamber temperature of around 700 °C to reduce the temperature gradient during the process. The slower speed and higher power were used for the melting process. Further details of the EBM processing could be found elsewhere.[24]

For microstructural analysis, crystallographic samples were collected and prepared from the XZ planes from all three samples as shown in Figure 1. A standard polishing process was used for preparing the crystallographic samples. The test coupons were polished gradually from coarse to the finer silicon carbide (SiC) grit sizes using various polishing equipment and grinders. Next, a low napped synthetic rayon polishing cloth and diamond suspensions with a particle size of 1, 0.25, and 0.1 μm, were used successively. Furthermore, a vibratory polishing was performed using 0.05 μm colloidal silica to get rid of the residual stresses and for obtaining a mirror surface finish. The samples were cleaned properly using soap solution and acetone between the steps to prevent the carriage of coarser particles to the next level. During the finer polishing steps, it is very difficult to remove the scratches from the previous steps. Therefore, before moving to the next step all samples were cleaned using ultrasound sonication in acetone solution. Finally, after the vibratory polishing, all samples were further cleaned in an ultrasound sonicator using acetone, methanol, and isopropyl alcohol (IPA) respectively before conducting EBSD analysis on them.

III. EXPERIMENTAL PROCEDURES

A. *Mechanical Property Measurements*

The high-temperature mechanical properties of as-built EBM Ti6Al4V samples were extracted from tensile testing at three different temperatures; 200 °C, 400 °C, and 600 °C. Three samples from each orientation were tested at a particular temperature and the average values were taken for the various mechanical properties such as young's modulus, yield strength, ultimate tensile strength, and percent elongation. The tensile tests were performed using an MTS Criterion® Electromechanical Universal Test System named MTS C45 at strain rate control mode and with a strain rate of 0.05 mm/mm/min. The strain was measured using an Epsilon® axial extensometer with a gauge length of

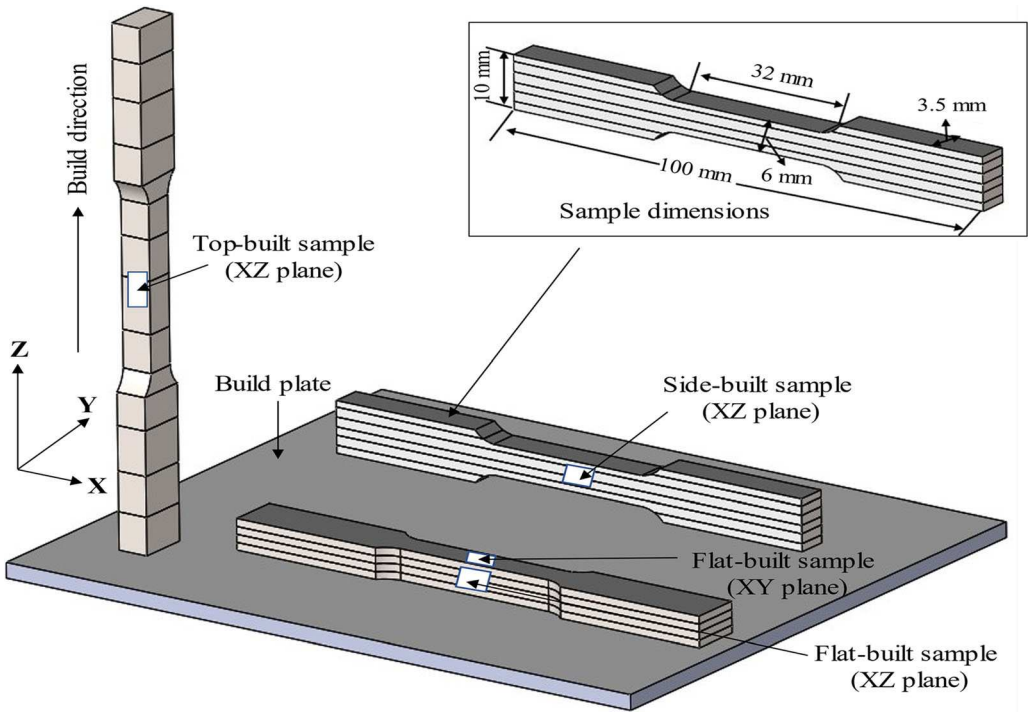

Fig. 1—CAD design with orientations on the build table and dimensions (inserted image) of the sub-sized dog-bone shaped Ti6Al4V tensile specimens for the EBM process. The location of the crystallographic test coupons extracted for the microstructural analysis is marked with a white box.

10 mm. The system is equipped with a convection chamber. The temperature inside the environmental chamber was controlled using Eurotherm® 2404 temperature controller. Further details of the high-temperature mechanical behaviors and their underlying mechanisms analysis could be found elsewhere.[24] The surface roughness, internal porosity, hardness, and tensile properties at room temperature were measured on the three different samples to examine how they vary with the orientations. The microstructural analysis was also performed on the as-built samples before tensile testing to understand their effect on the anisotropic mechanical behaviors inherent to the PBF AM process.[25,26] This study focuses on change in the deformation mechanisms and resulting microstructure due to anisotropy and combined high temperatures and mechanical loading.

B. *Microstructural EBSD Analysis*

The electron backscatter diffraction (EBSD) analysis was conducted on the samples after tensile testing to observe the changes in their crystallographic textures, preferred grain orientations, grain sizes, and grain boundary misorientation angles with various temperatures. The effect of the microstructural changes on the subsequent mechanical behaviors has been studied. The observed softening behaviors in terms of flow stress properties have been investigated as well from the related microstructural changes. The EBSD scans were accomplished using a ZEISS FIB-SEM SEM instrument equipped with EDAX®|AMETEK® EBSD detector. The focused electron beam was emitted at the prepared sample at 20 kV, with a high current mode, and an aperture size of 120 μm. The sample was tilted at 70 degrees with the source beam to capture the backscattered electron. The EBSD Kikuchi bands from the generated backscattered electrons were captured using the detector and a computer interface. The 500× magnification was used for capturing EBSD images from different samples. The scan area was 175 × 175 μm with a step size of 0.1 μm. The total dwell time for each of the scans was around 3 to 4 hours. Furthermore, the OIM Analysis v8 software was used for analyzing the scanned images and obtaining various grains maps and microstructural information. Further details could be found elsewhere.[26]

IV. RESULTS AND DISCUSSION

A. *High-Temperature Mechanical Softening Behaviors*

As it appears from the stress strain data shown in Figure 2, strength and ductility are inversely affected by the build orientations. While flat-built sample displayed superior strength both room temperature and high temperatures it exhibited lower ductility than other orientations and as compared to the conventionally manufactured parts as shown in Table I. The flat-built sample showed strength and modulus properties comparable with the conventional wrought Ti6Al4V alloys.[27,28] While, both the side-built and top-built samples showed larger ductility than the flat built samples, their other properties are either similar or considerably lower than their traditional wrought or conventionally manufactured counterpart. A summary of the properties found in literature are provided in Table I.

Various mechanical properties such as yield strength, modulus of elasticity, ultimate tensile strength and percent elongation of EB-PBF built Ti6Al4V parts change significantly with the increasing test temperatures as shown in Figure 2 for all three build orientations. All the samples showed considerable temperature dependency as can be observed from the representative engineering stress–strain curves of the samples. Intuitively, ductility increases with increasing the temperature, and material softens, hence lower strength at higher temperatures. At 600 °C, a significant decrease of flow stress and consequent softening behavior was observed at all three different orientations.

However, there was significant strain/work hardening observed in the plastic region of the curves at room temperature, 200 °C, and 400 °C. Dislocation entanglements and their interaction with the barriers such as the grain boundaries and other dislocations are the most dominant strain hardening mechanisms in the majority of the metals.[34] However, there is a significant change in the flow stress behavior when the temperature increases from 200 °C to 400 °C. There is a considerable decrease in percent elongation at 400 °C in top built and side-built samples. For this alloy, possible formation of Ti_3Al could result in hardening and decrease in ductility. Further analysis may be required to conform formation of this intermetallic phase. Although the significant loss of ductility has been reported in literature in Ti alloys at temperatures above 1000 °C,[35] the fundamental mechanisms causing this loss may be attributed more to the anisotropy of the material. The EBM-built Ti6Al4V samples display significant softening or hot working behaviors at 600 °C. Various mechanisms such as grain growth,[14] change of phases, grain boundary slip, dislocation glides,[36] dynamic recrystallization (DRX),[13,14] and globularization,[15,37,38] coarsening, elongation, and rotation of alpha phase[19,39] are generally found to be responsible for softening of titanium alloy depending on the temperature and manufacturing processes. The phase transformation and DRX mechanisms are more prominent at $\alpha + \beta$ phase-field temperature (between 850 °C and 950 °C). Whereas, both dynamic recovery (DRV) and DRX could be observed at temperatures larger than the β-transus (995 °C).

SEM images of the fractured surface is provided in Figure 3. Various internal defects like pores, keyholes, and un-melted powder particles, as can be seen in these figures. These defects can initiate or accelerate the crack propagation and thus degrade the mechanical properties. At all three temperatures, the flat-built samples display a smoother fracture surface than the other two orientations, while the top-built samples have the roughest fracture surface because of longer plastic deformation. With the increasing temperature, fracture surfaces become rougher for any orientation as well.

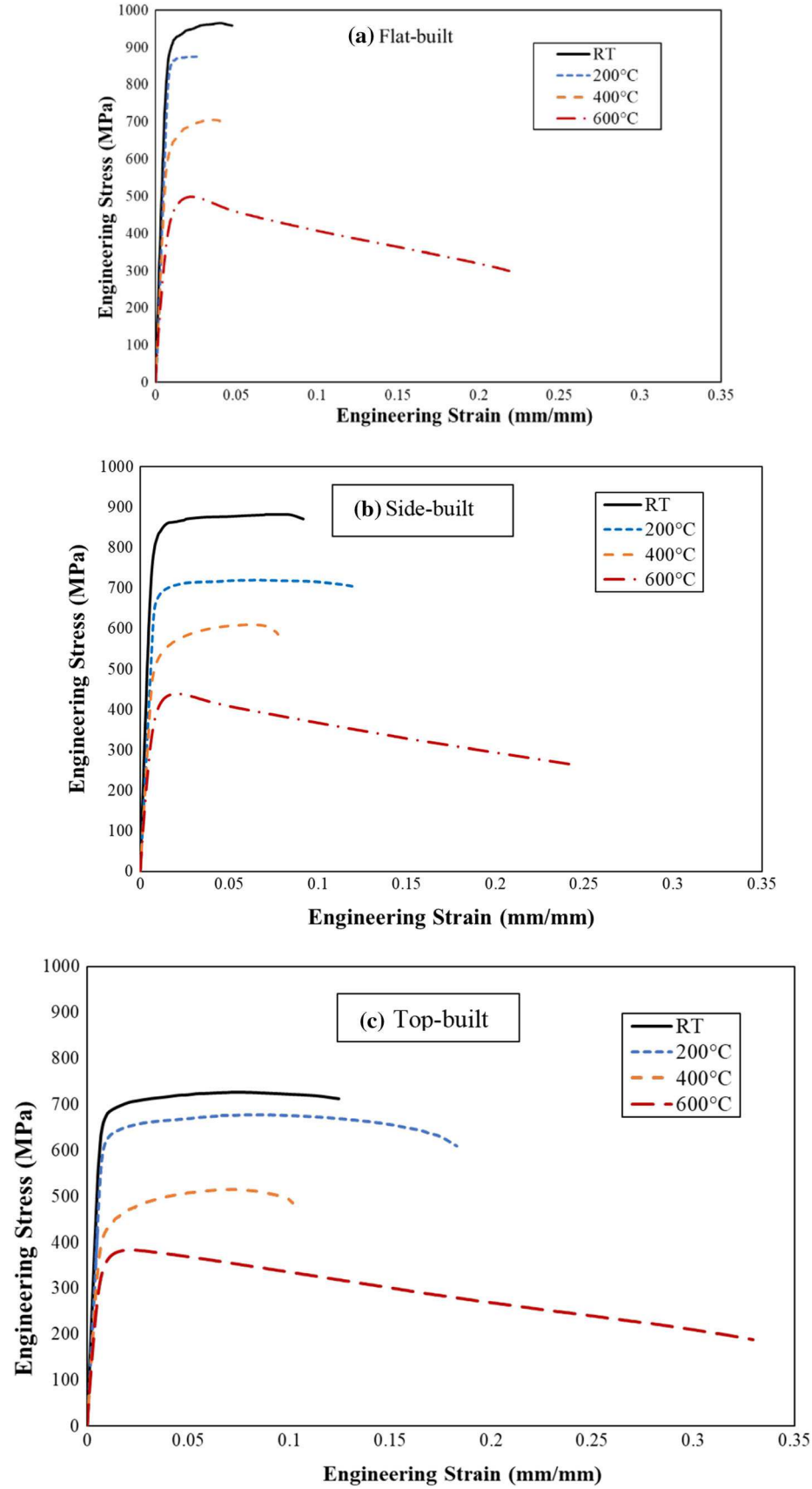

Fig. 2—Engineering stress–strain curves of EBM Ti6Al4V (*a*) flat-built, (*b*) side-built, and (*c*) top-built samples, tested at room temperature (RT), 200 °C, 400 °C, and 600 °C temperatures and exhibiting softening behaviors at 600 °C temperature.

B. *Microstructural Analysis Before Tensile Testing*

A microstructural analysis on as-built EBM Ti6Al4V samples was conducted before the tensile test to understand the potential reasons for the observed anisotropic mechanical behaviors among the samples built in different orientations. The inverse pole figure maps (Figure 4) confirm that the microstructure of EBM-built Ti6Al4V parts is consist of mainly α phases (α colony and α basketweave) and prior β phases which are distributed among the grain boundaries of alpha phases. Both the flat-built and side-built samples were observed to have alpha grains preferably orientated in the < 11 and $\langle 11\bar{2}0\rangle$ directions, while the preferred orientation of the top-built sample was inclined to the <0001> direction, while a significant number of grains were orientated to the $\langle 10\bar{1}0\rangle$ direction. The average grain sizes of the flat-built, side-built, and top-built samples were found to be 4.1, 5.3, and 6.6 μm, respectively, whereas, the average grain boundary misorientation angles were 25.7, 23.7, and 22.9 degrees, respectively. Furthermore, the flat-built sample had an area fraction of β phase of around 3.3 pct and α phase of 96.7 pct on the scanned area. However, the area fraction of the β phase was observed to increase to 5.1 and 9.0 pct for the side-built and top-built samples, respectively. Multiple factors could have an impact on these values. Faster cooling can result in higher percentage of prior β phase remaining in the material as the nonequilibrium condition does not allow for complete transformation of the β phases. However, other factors that are associated with anisotropic formation of grains can also impact the percentage of the β phase that is observed in the EBSD imaging. For example, the columnar grain growth can determine the texture and percentage of the grain boundaries that are present in the EBSD image. Therefore, this slight difference in β phase ratio can be attributed to the anisotropic formation of grains.

The higher percentage of β phase, which is comparatively softer than the α phase,[13,15,40] could potentially impact the overall strength of the material, although this difference in our case is minimal, their increased ratio could have slight contribution in ductility observed in the top built samples. Similarly, as the ratio of α phase is higher in flat-built sample, this orientation has shown higher strength than other two orientations. These observed variations in preferred grain orientation, grain sizes, and grain boundary misorientation angles were anticipated to be due to the variation of the geometry of the three samples, subsequent changes in the thermal gradient and cooling rates during the solidification process, and thermal annealing phenomena due to an elevated build chamber temperature.[41] Therefore, the strong microstructural variation in different orientations was found to mainly dictate the mechanical anisotropic behaviors of the EBM-built Ti6Al4V parts.

C. *Evolution of Microstructure with Thermomechanical Loading*

The EBSD inverse pole figure (IPF) maps of the top-built samples after tensile testing at 200 °C, 400 °C, and 600 °C temperatures are presented in Figure 5. In all cases significant decrease in the flow stress is observed at higher temperatures as seen in Figure 2. The increased dislocation mobility due to increased temperatures could be the potential reason for lower mechanical properties obtained at higher temperatures as compared to the room temperature properties. The IPF maps shown in Figure 5 don't show a significant distinguishable difference between the grain orientations at different temperatures. In all three different temperatures, there seems to be regions of the materials that have preferred grain orientations.

Given that the plane that is being examined in top built samples are parallel to the build orientation and parallel to the loading direction. This could be observed through the texture very clearly in the IPF map of mechanical test at 600C. The grains look stretched out and elongated after going through the tensile testing at 600 °C because of the applied thermomechanical loading. From the IPF maps it looks as the grains are oriented in $\langle 0001\rangle$ and $\langle 10\bar{1}0\rangle$.

The variation of grain sizes with the increasing temperatures can be further observed from the grain size distribution curves of the three top-built samples tested at three temperatures as presented in Figure 6. The top-built sample tested at 200 °C has an almost identical grain size distribution curve as the sample before undergoing any deformation loading. The average grain size of this sample is around 6.6 μm.. The sample tested at 400 °C displayed an increase of the grain size distribution with a maximum grain of 23 μm and an average grain size of 7.1 μm. whereas, the top-built sample tested at 600 °C showed a significant shift of the grain distribution curve to the right, reaching a maximum grain size of 32 μm and average grain size of 8.8 μm. These further indicate the grain growth and coarsening as various softening mechanisms are activated at this elevated temperature.

The misorientation angle distributions of the top-built samples after tensile loading at 200 °C, 400 °C, and 600 °C are compared and presented in Figure 7. The average of misorientation angles decreases from 22 degrees to 20.5 and 19 deg with increasing temperatures from 200 °C to 400 °C and 600 °C, respectively. The number fractions of low angle grain boundaries (LAGBs, < 15 deg) decreases with increasing temperatures. However, this high angle boundaries larger than 55 deg show an increase with increasing temperature. This variation of misorientation angle could potentially show dissolution of low angle grains to form new grains, which may be due to geometric deformation of the grains at higher temperatures.[42–44]

Table I. Mechanical Behaviors of Conventional Ti6Al4V Parts Available at Literature

Sample Type	Temp. (°C)	E (GPa)	σ_y (MPa)	UTS (MPa)	Elongation (Pct)	Strain Rate (s^{-1})	References
Ti6Al4V (Wrought)	RT	105–107	860–962	930–1008	> 10	8×10^{-4}	[27–29]
Ti6Al4V (Conventional)	500	NA	436	467	31.2	8.3×10^{-3}	[30]
	RT		968	1015	12		
Ti6Al4V (CHIP)	538	NA	356	430	13.4	6.7×10^{-5}	[31]
			382	463	15.5	6.7×10^{-4}	
Ti6Al4V (Hot-Rolled)	700	NA	580	NA	NA	8×10^{2}	[32]
	RT		998				
Ti6Al4V (Cold Rolled)	450	NA	505	592	28	6.6×10^{-4}	[33]
	RT		903	982	19		

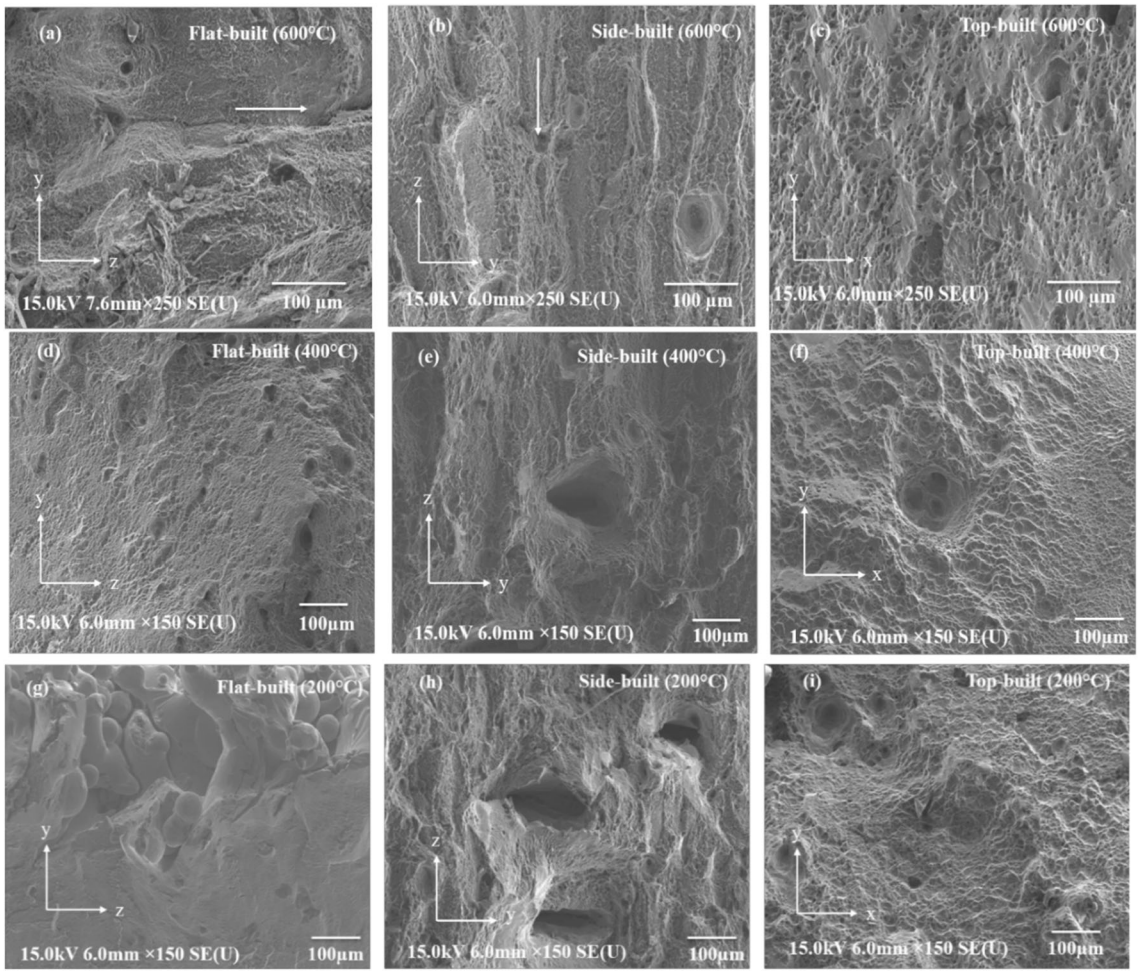

Fig. 3—Secondary Electron Microscopy (SEM) images with coordinate systems of the fracture surfaces (taken at mid-cross section) of as-built EBM Ti6Al4V, (*a*, *b* and *c*) flat-built, side-built, and top-built samples tested at 600 °C, (*d*, *e* and *f*) flat-built, side-built, and top-built samples tested at 400 °C, and (*g*, *h* and *i*) flat-built, side-built, and top-built samples tested at 200 °C.

The evolution of the texture of the grains of the top-built Ti6Al4V samples after tensile testing at 200 °C, 400 °C, and 600 °C are presented *via* both alpha and beta pole figures as presented in Figure 8. The maximum intensity of harmonic texture of the beta pole figures decreases from 6.27 to 2.79 with increasing temperatures from 200 °C to 600 °C. Whereas, the maximum intensity of the harmonic texture of the alpha pole figures increases from 7.04 to 12.32 with increasing temperature from 200 °C to 600 °C. The intensities of the different preferred grain orientations which are $\langle 0001 \rangle$, $\langle 11\bar{2}0 \rangle$ and $\langle 11\bar{2}1 \rangle$ changed considerably following the tensile testing at different temperatures as visible from the α pole figure harmonic texture maps in Figure 8(a).

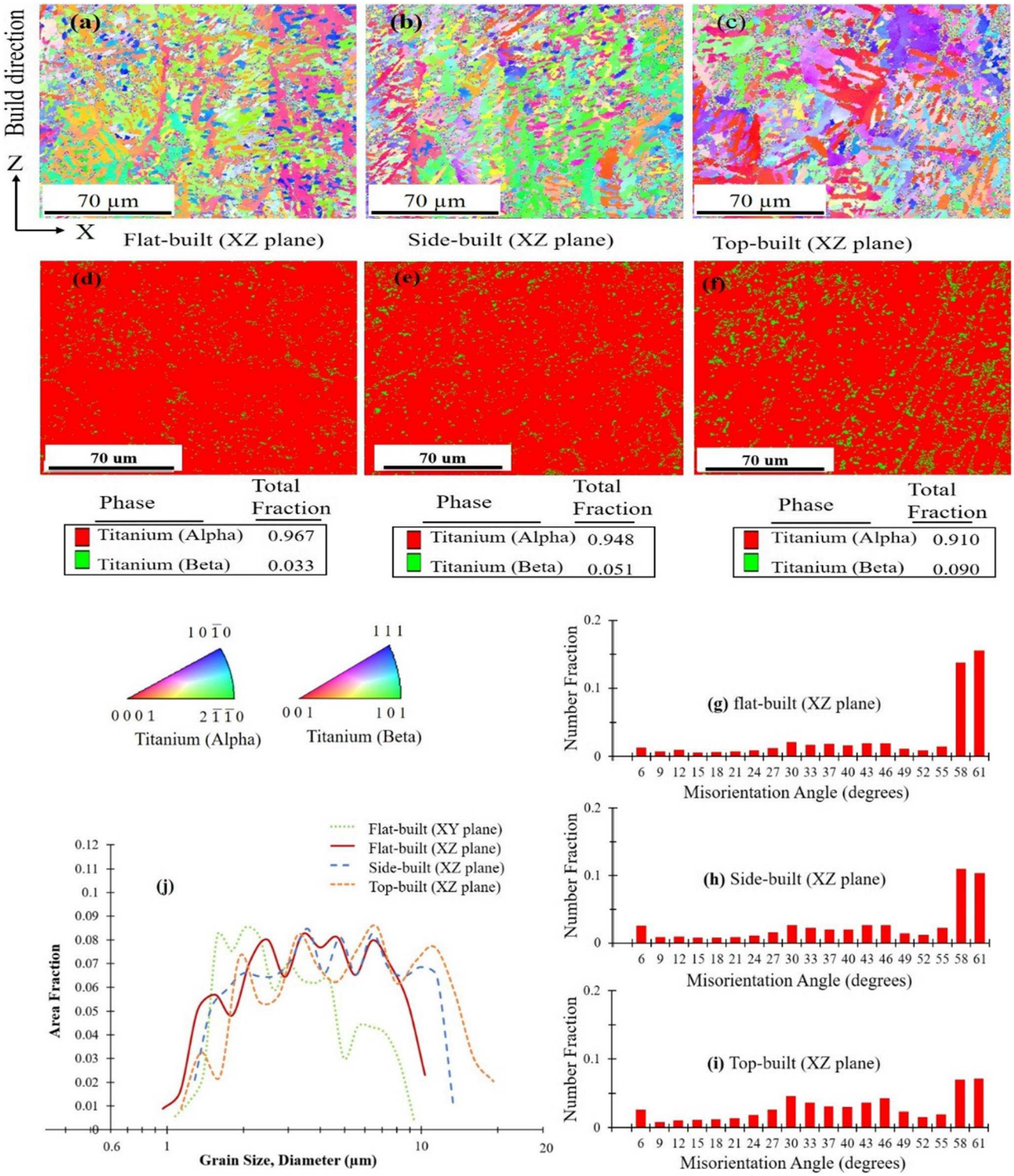

Fig. 4—Various EBSD maps of the three Ti6Al4V samples. The top three inverse pole figure (IPF) maps show different preferred grain orientations on the three samples, (*a*) flat-built, (*b*) side-built, (*c*) top-built. While phase maps (*d–f*) show prior beta phases in between the alpha grain boundaries of flat-built, side-built, and top-built samples, respectively. The (*g–i*) show misorientation angle distribution curves, and (*j*) shows the grain size distribution curves of the three samples.

Similarly, the side-built EBM Ti6Al4V samples also exhibit the evolution of the grain size, texture, and phases with the increment of tensile testing temperature. The EBSD IPF maps of the three side-built samples after tensile testing at 200 °C, 400 °C and 600 °C temperature as presented in Figure 9 clearly show the change of microstructural features with increasing temperature. The grain growth and distortion of the

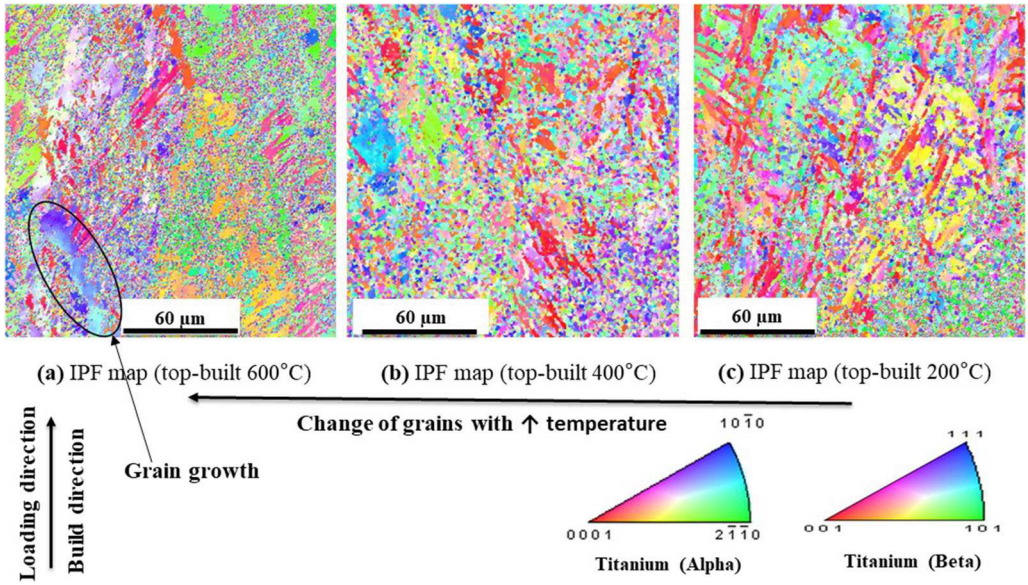

Fig. 5—The EBSD IPF maps of top-built samples after tensile testing at (*a*) 600 °C, (*b*) 400 °C, and (*c*) 200 °C temperatures, exhibiting possible grain growth, distortion, and grain boundary slip as potential softening mechanisms.

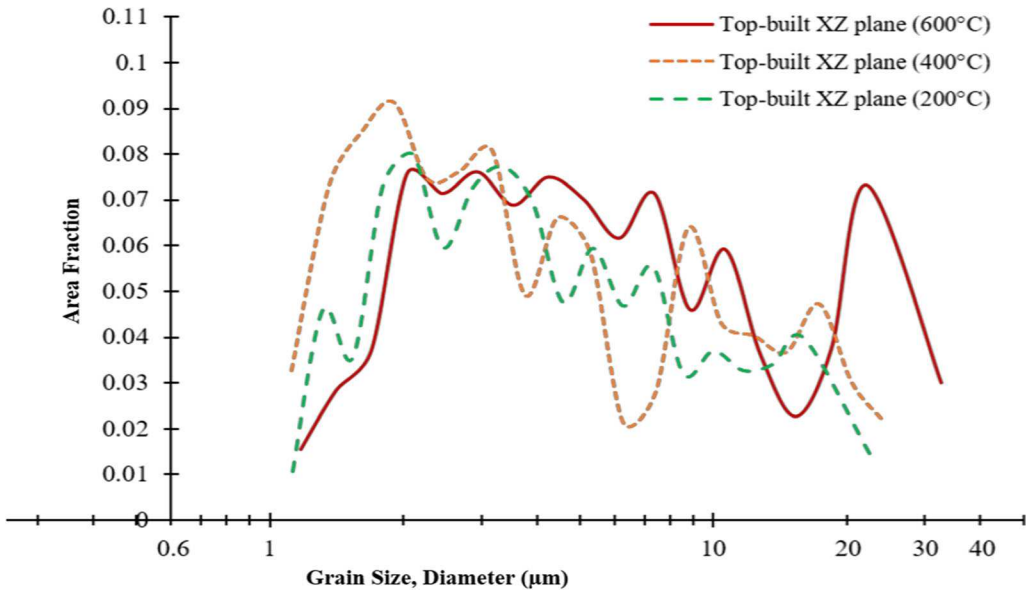

Fig. 6—Grain size distributions of top-built samples at *XZ* plane after tensile testing at 200 °C, 400 °C, and 600 °C temperature respectively, showing the evolution of grain sizes and grain growth with an increment of testing temperatures.

alpha grain boundary could be observed as the temperature increases from 200 °C to 600 °C. Larger alpha grains could be noticed for the side-built Ti6Al4V sample after deformation at 600 °C (Figure 9(a)) The grain distribution seems to be more uniform at 200 deg, while at higher temperatures the distribution seems to have shifted in a way that larger aeras with specific grain orientation are observed. At 400 deg, this grain seems to be oriented in $\langle 10\bar{1}0 \rangle$ orientation while at 600 °C this preferred orientation seems to have tilted more toward $\langle 001 \rangle$ orientation. The distribution of grain sizes of the side-built samples tested at the three temperatures is presented in Figure 9(d). The grain size distribution curves of the samples tested at 200 °C and 400 °C have a slight difference. The former has a maximum grain size of 14 μm and an average grain size of 5.3 μm. At 400 °C, the side-built Ti6Al4V sample has a maximum grain size of 16 μm and an average grain size of 6.2 μm. While the side-built sample tested at 600 °C has a noticeable difference in grain distribution curve when compared with the curves of the former two samples. The sample after going through deformation at 600 °C,

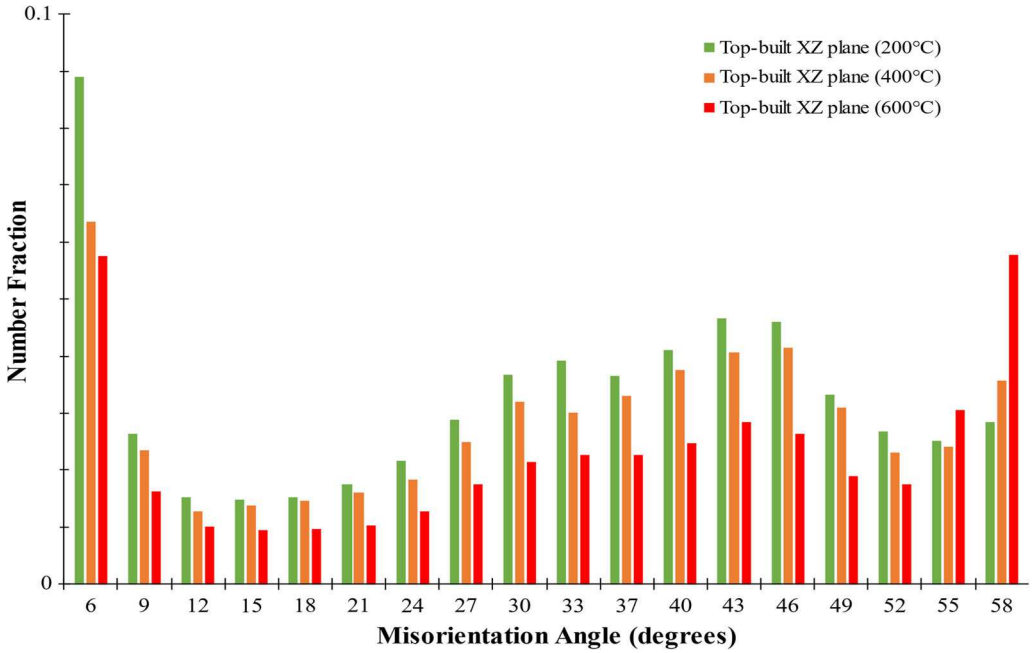

Fig. 7—Misorientation angle distributions of top-built samples at XZ plane after tensile testing at 200 °C, 400 °C, and 600 °C temperatures respectively.

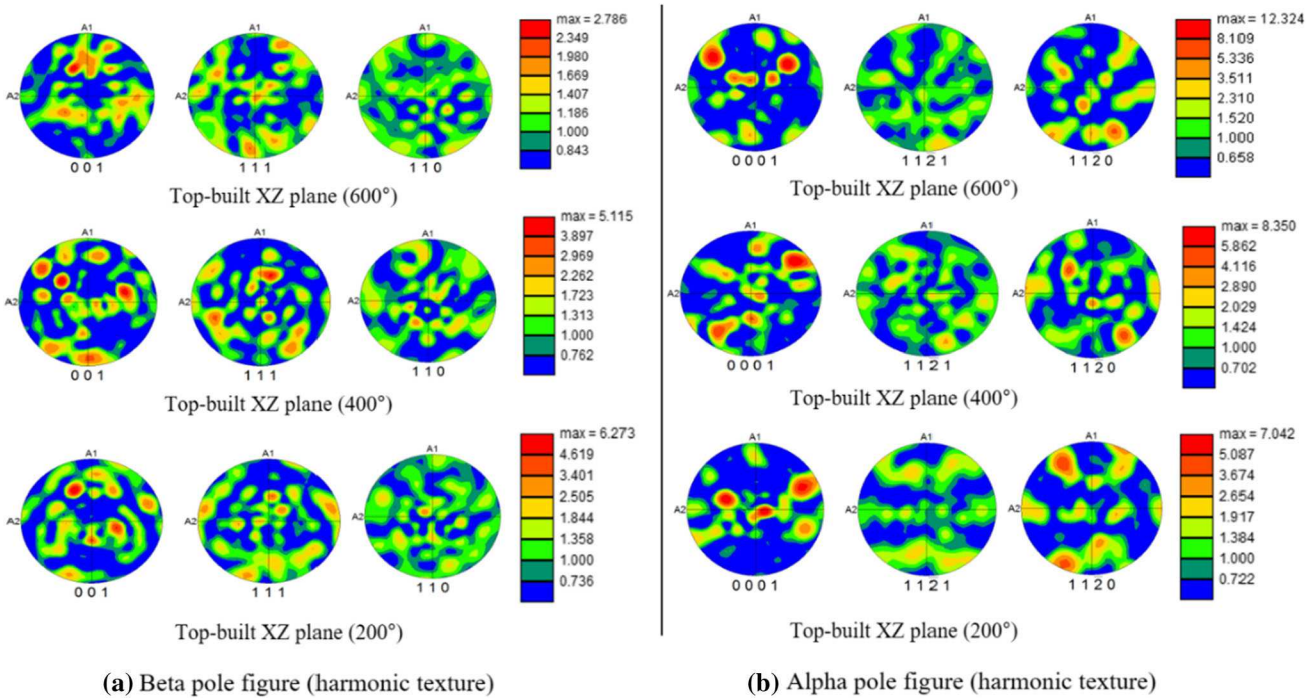

Fig. 8—Harmonic texture of (*a*) beta pole figure and (*b*) alpha pole figure of the top-built samples on XZ plane, after tensile testing at 600 °C, 400 °C, and 200 °C temperature, respectively. The maximum texture intensity of beta is decreasing, and alpha is increasing with increasing temperature.

acquire elongated and coarser grains as large as 21 μm in diameter and with an average size of around 7.8 μm.

However, the intensity of the grain texture changes with the testing condition as can be seen from the alpha and beta pole figures in Figure 10. The maximum intensity of the alpha pole figure increases slightly with increasing temperature. In the case of the beta pole figure, it increases from 200 °C to 400 °C and again decreases at 600 °C temperature. These changes are not very significant.

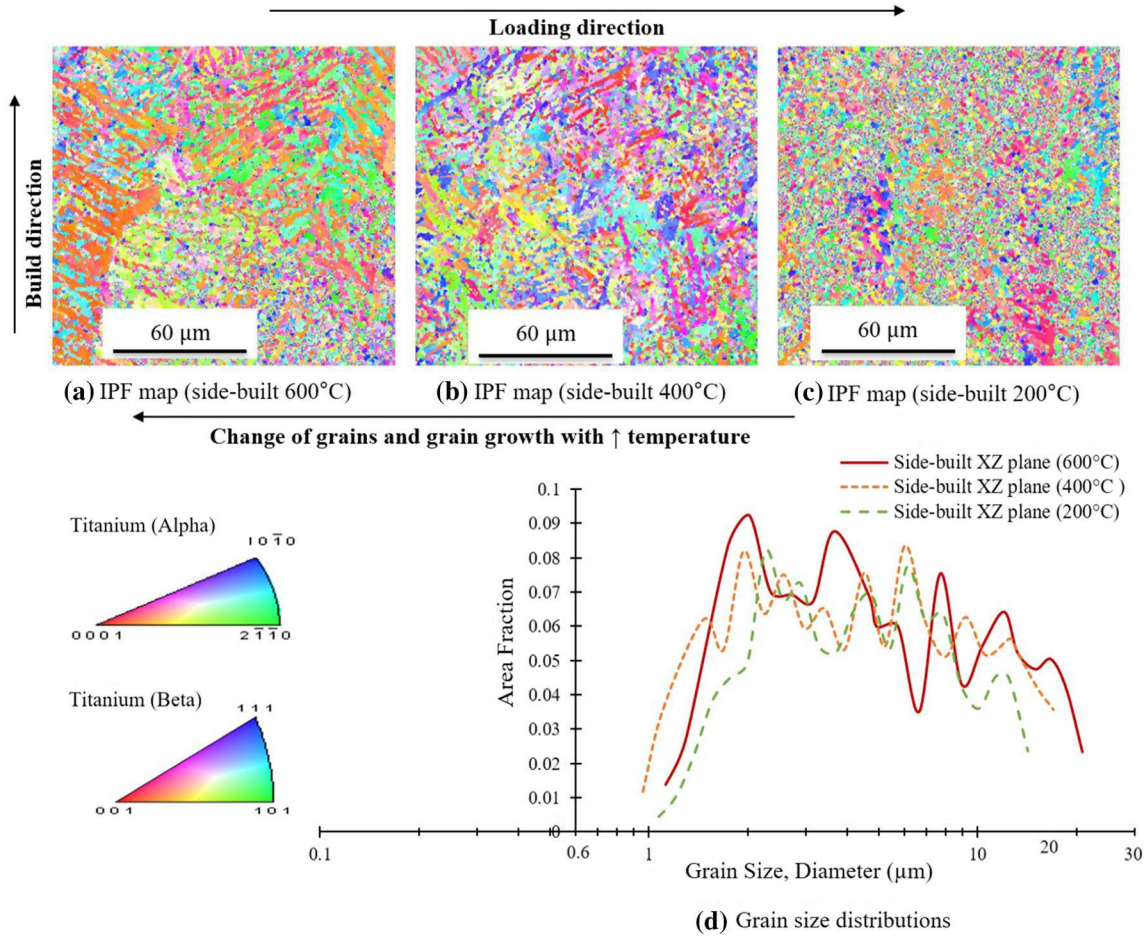

Fig. 9—EBSD IPF maps of the side-built samples after tensile testing at (*a*) 600 °C, (*b*) 400 °C, and (*c*) 200 °C temperatures, exhibiting a change of grains, grain growth, distortion, and grain boundary slip as potential softening mechanisms. And (*d*) drain size distribution graphs showing the evolution of grain sizes and grain growth with an increment of testing temperatures.

V. CONCLUSION

The microstructural analysis of Ti6Al4V samples built using electron beam melting PBF AM process showed the presence of both α phase and β phase. More than 90 pct of the grains consist of the α phase, whereas, there is a very small amount of β phases distributed at the grain boundaries of the α matrix. The variation of the preferred orientation of the grains due to the variation of the cooling rates and thermal gradient in various samples with different orientations mainly contributed to the anisotropic mechanical behaviors. All the samples showed significant temperature sensitivity when tensile tested at different high temperatures up to 600 °C. Though significant strain/work hardening was observed at the plastic region of the stress and strain curves obtained at room temperature, 200 °C, and 400 °C temperatures, EBM built Ti6Al4V samples displayed significant softening or hot working behaviors at 600 °C.

The grains size increased noticeably in all orientations. This was mainly associated with geometric deformation where low angle grain boundaries dissolved and formed larger grains.. For example, in the case of the vertically built sample, the maximum initial grain size increased from 19 to 32 μm after tensile testing at 600 °C temperature. When compared the misorientation angles of different samples, fraction of LAGBs (< 15 deg) decreases with increasing temperature. This geometric deformation and grain coarsening could potentially be the cause of the softening observed at higher temperatures. The maximum intensity of harmonic texture decreases from 6.27 to 2.79 for beta pole figures and increases from 7.04 to 12.32 for alpha pole figures with increasing temperature from 200 °C to 600 °C in the vertically built samples.

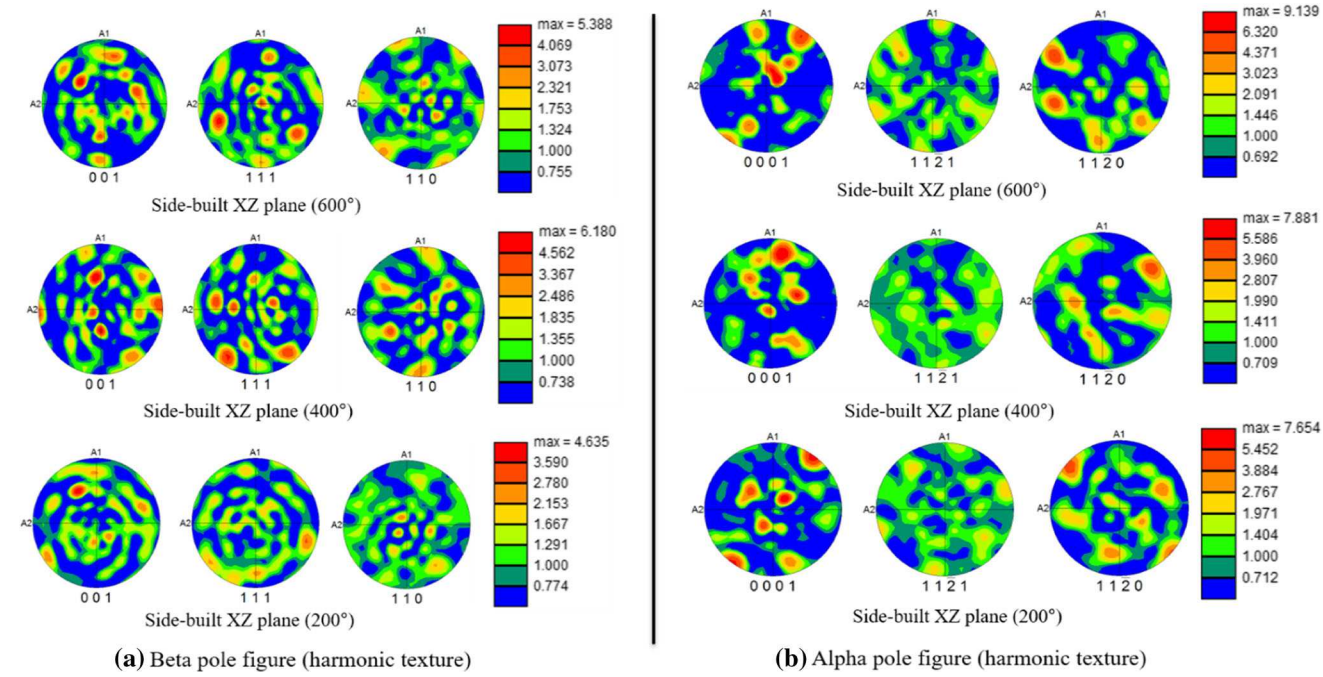

(a) Beta pole figure (harmonic texture)

(b) Alpha pole figure (harmonic texture)

Fig. 10—Harmonic texture of (*a*) beta pole figure and (*b*) alpha pole figure of the side-built samples on *XZ* plane, after tensile testing at 600 °C, 400 °C, and 200 °C temperature, respectively. The maximum texture intensity of beta decreased from 400 °C to 600 °C, and the maximum intensity of alpha increased with increasing temperature.

ACKNOWLEDGMENTS

We acknowledge the use of facilities within the Eyring Materials Center at Arizona State University supported in part by NNCI-ECCS-2025490. Additionally, we would like to thank the ASU core facilities for providing the tools necessary for accomplishing the tasks. Furthermore, authors would like to thank NASA Marshal Space Flight Center for providing the printed parts.

AUTHOR CONTRIBUTIONS

LL: Conceptualization, methodology, formal analysis, investigation, re-writing of the whole paper, validation, resources, data curation, writing—review and editing, visualization, supervision, project administration, funding acquisition. JR: Conceptualization, validation, data curation, visualization, supervision, project administration. MJM: Software, validation, data curation, writing—original draft preparation, writing, visualization.

FUNDING

This research received no external funding.

DATA AVAILABILITY

Additional supporting data can be provided upon request.

CONFLICT OF INTEREST

The authors declare no conflict of interest.

REFERENCES

1. S. Liu and Y.C. Shin: *Mater. Des.*, 2019, vol. 164, 107552.
2. J.C. Najmon, S. Raeisi, and A.. Tovar: *Review of Additive Manufacturing Technologies and Applications in the Aerospace Industry*, Elsevier, 2019.
3. P. Nandwana and Y. Lee: *Mater. Today Commun.*, 2020, vol. 24, 100962.
4. L. Ladani, J. Razmi, and S.F. Choudhury: *J. Eng. Mater. Technol. Trans. ASME*, 2014, vol. 136, pp. 1–7.
5. H.K. Rafi, N.V. Karthik, H. Gong, T.L. Starr, and B.E. Stucker: *J. Mater. Eng. Perform.*, 2013, vol. 22, pp. 3872–83.
6. X. Zhou, N. Dai, M. Chu, L. Wang, D. Li, L. Zhou, and X. Cheng: *Int. J. Adv. Manuf. Technol.*, 2020, vol. 106, pp. 3–14.
7. V. Chastand, P. Quaegebeur, W. Maia, and E. Charkaluk: *Mater. Charact.*, 2018, vol. 143, pp. 76–81.
8. X. Wang, L. Wang, L.S. Luo, X.D. Liu, Y.C. Tang, X.Z. Li, R.R. Chen, Y.Q. Su, J.J. Guo, and H.Z. Fu: *J. Alloys Compd.*, 2017, vol. 728, pp. 709–18.
9. X. Tan, Y. Kok, Y.J. Tan, G. Vastola, Q.X. Pei, G. Zhang, Y.W. Zhang, S.B. Tor, K.F. Leong, and C.K. Chua: *J. Alloys Compd.*, 2015, vol. 646, pp. 303–09.
10. L. Ladani: *Metall. Mater. Trans. A Phys. Metall. Mater. Sci.*, 2015, vol. 46, pp. 3835–41.
11. B.E. Carroll, T.A. Palmer, and A.M. Beese: *Acta Mater.*, 2015, vol. 87, pp. 309–20.
12. X. Wang and K. Chou: *J. Alloys Compd.*, 2018, vol. 748, pp. 236–44.
13. R. Ding, Z.X. Guo, and A. Wilson: *Mater. Sci. Eng. A*, 2002, vol. 327, pp. 233–45.
14. L. He, A. Dehghan-Manshadi, and R.J. Dippenaar: *Mater. Sci. Eng. A*, 2012, vol. 549, pp. 163–67.

15. Q. Bai, J. Lin, T.A. Dean, D.S. Balint, T. Gao, and Z. Zhang: *Mater. Sci. Eng. A*, 2013, vol. 559, pp. 352–58.
16. C.H. Park, J.H. Kim, Y.T. Hyun, J.T. Yeom, and N.S. Reddy: *J. Alloys Compd.*, 2014, vol. 582, pp. 126–29.
17. P.M. Souza, P.D. Hodgson, B. Rolfe, R.P. Singh, and H. Beladi: *J. Alloys Compd.*, 2019, vol. 793, pp. 467–79.
18. S. Zherebtsov, M. Murzinova, G. Salishchev, and S.L. Semiatin: *Acta Mater.*, 2011, vol. 59, pp. 4138–50.
19. B. Babu and L.E. Lindgren: *Int. J. Plasticity*, 2013, vol. 50, pp. 94–108.
20. L. Ladani and M. Sadeghilaridjani: *Metals (Basel)*, 2021, vol. 11, p. 1391.
21. L. Ladani: *Additive Manufacturing of Metals, Materials, Processes, Tests and Standards*, DEStech, Lancaster, 2020.
22. ASTM E8: *Annual Book of ASTM Standards 4*, 2010, pp. 1–27.
23. Arcam: *GE Additive*, 2019, p. 2.
24. M.J. Mian, J. Razmi, and L. Ladani: *J. Manuf. Sci. Eng. Trans. ASME*, 2021, vol. 143, pp. 1–2.
25. M.J. Mian, J. Razmi, and L. Ladani: *Materialia*, 2021, vol. 16, 101041.
26. M.J. Mian, J. Razmi, and L. Ladani: *Metals (Basel)*, 2022, vol. 12, pp. 1–20.
27. M. Shunmugavel, A. Polishetty, and G. Littlefair: *Procedia Technol.*, 2015, vol. 20, pp. 231–36.
28. S. Lampman: *Properties and Selection: Nonferrous Alloys and Special-Purpose Materials*, 2018, vol. 2, ASM International, Materials Park, pp. 592–633.
29. GE: *GE Additive*, 2023, pp. 5–7.
30. J. Kim, K.H. Kim, and D. Kwon: *Met. Mater. Int.*, 2016, vol. 22, pp. 209–15.
31. J.H. Zhu, P.K. Liaw, J.M. Corum, and H.E. McCoy: *Metall. Mater. Trans. A Phys.*, 1999, vol. 30, pp. 1569–78.
32. W.S. Lee and C.F. Lin: *Mater. Sci. Eng. A*, 1998, vol. 241, pp. 48–59.
33. S.H. Wang, M.D. Wei, and L.W. Tsay: *Mater. Lett.*, 2003, vol. 57, pp. 1815–23.
34. International Atomic and Energy Agency: *Non-Destructive Testing: A Guidebook for Industrial Management and Quality Control Personnel*, International Atomic and Energy Agency, Vienna, 1999.
35. B.B. Rath, B.K. Damkroger, M.A.. Imam and G.R. Edwards: *High Temperature Ductility Loss in Titanium Alloys—A Review*, Washington, DC (United States), 1994.
36. G.Z. Quan, G.C. Luo, J.T. Liang, D.S. Wu, A. Mao, and Q. Liu: *Comput. Mater. Sci.*, 2015, vol. 97, pp. 136–47.
37. I. Weiss, F.H. Froes, D. Eylon, and G.E. Welsch: *Metall. Trans. A*, 1986, vol. 17A, pp. 1935–47.
38. N. Stefansson and S.L. Semiatin: *Metall. Mater. Trans. A Phys. Metall. Trans. A*, 2003, vol. 34A, pp. 691–98.
39. T. Kurzynowski, M. Madeja, R. Dziedzic, and K. Kobiela: *Scanning*, 2019, vol. 2019, p. 12.
40. I. Weiss and S.L. Semiatin: *Mater. Sci. Eng. A*, 1999, vol. 263, pp. 243–56.
41. A.A. Antonysamy, J. Meyer, and P.B. Prangnell: *Mater. Charact.*, 2013, vol. 84, pp. 153–68.
42. S.V.S. Narayana Murty, N. Nayan, P. Kumar, P. Ramesh Narayanan, S.C. Sharma, and K.M. George: *Mater. Sci. Eng. A*, 2014, vol. 589, pp. 174–81.
43. Y. Kim, Y.B. Song, S.H. Lee, and Y.S. Kwon: *J. Alloys Compd.*, 2016, vol. 676, pp. 15–25.
44. J.J. Burke and V. Weiss: *Advances in Deformation Processing*, Plenum, New York, 1978.